Available online at www.sciencedirect.com
SCIENCE DIRECT
Trans. Nonferrous Met. Soc. China 18(2008) 930−937
Transactions of Nonferrous Metals Society of China
www.csu.edu.cn/ysxb/

Microscopic phase-field simulation for precipitation behavior of Ni-Al-Cr alloy during two-step aging

ZHANG Ji-xiang(张济祥), CHEN Zheng(陈 铮), LIANG Min-jie(梁敏洁), WANG Yong-xin(王永欣), LAI Qing-bo(来庆波)

School of Materials Science and Engineering, State Key Laboratory of Solidification Processing, Northwestern Polytechnical University, Xi'an 710072, China

Received 22 August 2007; accepted 21 April 2008

Abstract: Based on the microscopic phase-field model, the pre-aging temperature effects on the precipitation mechanism and microstructure evolution during two-step aging for $Ni_{75}Al_9Cr_{16}$ alloy were simulated. The results show that the early precipitation mechanism of $L1_2$ phase is the mixed mechanism of spinodal decomposition and non-classical nucleation growth, whereas the early precipitation mechanism of DO_{22} phase is spinodal decomposition when the pre-aging temperature is 873 K. The early precipitation mechanism of $L1_2$ phase is non-classical nucleation growth, whereas the early precipitation mechanism of DO_{22} phase is spinodal decomposition when the pre-aging temperature is 973 K. Under the effects of elastic strain energy, the cubic particles exhibit directional alignment along [100] and [010] directions during the late precipitation, which is more obvious at lower pre-temperature. DO_{22} phases appear earlier than $L1_2$ phases under these two kinds of precipitation processes; and the nucleation incubation time becomes long with the increase of pre-temperature.

Key words: Ni-Al-Cr alloy; precipitation mechanism; order parameter; microscopic phase-field; two-step aging

1 Introduction

Nowadays, Ni-Al-Cr alloys are the most important materials used in the advanced aero-engine and industrial gas turbine[1]. The precipitation process of Ni-Al-Cr alloys has been widely investigated by many scholars, however, which mainly focused on the modulation structure and pattern at the late stage of precipitation[2−5]. The macroscopic performance and behavior of alloy depend almost entirely on its microstructure. The size and distribution of precipitated phase particles can be controlled by the reasonable aging thermal treatment, thus, the better performance can be acquired for precipitation-strengthened alloys. The existent experimental methods are very difficult to clarify the early precipitation mechanism, therefore, the computer simulation and model application become more and more important in materials science.

Microscopic phase-field kinetic model has been successfully used in simulating the precipitation process in Al-Li[6], Ni-Al[7] and Ni-Al-V[8−10] alloys, which has shown considerable advantages, especially in highly non-linear and non-equilibrium kinetic systems. There is no need to assume the phase structure or precipitation mechanism of new phase beforehand and the interatomic interactions within the system are the only input variables. The initial state of alloy is a homogeneous disordered state; and the information of phase structure, microstructure and order parameter is obtained by the change of atomic occupation probabilities resulted from atomic transition. The main objective of this work is to theoretically investigate and clarify the pre-aging temperature effects on the precipitation mechanism and microstructure during two-step aging for $Ni_{75}Al_9Cr_{16}$ alloy by microscopic phase model, in which atom figures and order parameters are applied.

2 Theoretical model

Microscopic diffusion equation developed by KHACHATURYAN[11] is actually the microscopic style

Foundation item: Project(50671084) supported by the National Natural Science Foundation of China; Project(Z200714) supported by the Postgraduate Foundation of Northwestern Polytechnical University, China
Corresponding author: ZHANG Ji-xiang; Tel: +86-29-88474095; E-mail: zhangjixiangdoctor@yahoo.com.cn

of Cahn-Hilliard equation. In this model, the atomic configuration and the morphologies of a ternary alloy are described by a single-site occupation probability function, $P_A(\boldsymbol{r}, t)$, $P_B(\boldsymbol{r}, t)$ and $P_C(\boldsymbol{r}, t)$ which represent the probabilities of finding an A, B or C atom at a given lattice site r at a given time t, respectively. Since for ternary systems $P_A(\boldsymbol{r}, t)+ P_B(\boldsymbol{r}, t)+ P_C(\boldsymbol{r}, t)=1.0$, only two equations are independent at each lattice. If one assumes the independent variables are $P_A(\boldsymbol{r}, t)$ and $P_B(\boldsymbol{r}, t)$, there will be two independent kinetic equations at each lattice site for species A and B, respectively. Then, one can write the microscopic kinetic equations for ternary systems as

$$\begin{cases} \dfrac{\mathrm{d}P_A(\boldsymbol{r},t)}{\mathrm{d}t}=\dfrac{1}{k_BT}\sum\limits_{\boldsymbol{r}'}\Big[L_{AA}(\boldsymbol{r}-\boldsymbol{r}')\dfrac{\partial F}{\partial P_A(\boldsymbol{r}',t)}+ L_{AB}(\boldsymbol{r}-\boldsymbol{r}')\dfrac{\partial F}{\partial P_B(\boldsymbol{r}',t)}\Big]+\zeta(\boldsymbol{r},t) \\ \dfrac{\mathrm{d}P_B(\boldsymbol{r},t)}{\mathrm{d}t}=\dfrac{1}{k_BT}\sum\limits_{\boldsymbol{r}'}\Big[L_{BA}(\boldsymbol{r}-\boldsymbol{r}')\dfrac{\partial F}{\partial P_A(\boldsymbol{r}',t)}+ L_{BB}(\boldsymbol{r}-\boldsymbol{r}')\dfrac{\partial F}{\partial P_B(\boldsymbol{r}',t)}\Big]+\zeta(\boldsymbol{r},t) \end{cases} \tag{1}$$

where $L_{\alpha\beta}(\boldsymbol{r}-\boldsymbol{r}')$ is the exchange probability between a pair of atoms, α and β, at lattice site $\boldsymbol{r}$ and $\boldsymbol{r}'$ per unit time, α, β=A, B or C; F is the total Helmholtz free energy of the system; T is the temperature and k_B is the Boltzmann constant; and $\zeta(\boldsymbol{r}, t)$ is thermal noise which is assumed to be Gaussian-distributed with the average value of zero.

In the mean field theory, the free energy F is approximately given by

$$\begin{aligned} F=&-\frac{1}{2}\sum_{\boldsymbol{r}}\sum_{\boldsymbol{r}'}\Big[V_{AB}(\boldsymbol{r}-\boldsymbol{r}')P_A(\boldsymbol{r})P_B(\boldsymbol{r}')+ V_{BC}(\boldsymbol{r}-\boldsymbol{r}')P_B(\boldsymbol{r})P_C(\boldsymbol{r}')+V_{AC}(\boldsymbol{r}-\boldsymbol{r}')P_A(\boldsymbol{r})P_C(\boldsymbol{r}')\Big]+ \\ &\boldsymbol{k}_BT\sum_{\boldsymbol{r}'}\Big[P_A(\boldsymbol{r})\ln\big(P_A(\boldsymbol{r})\big)+P_B(\boldsymbol{r})\ln\big(P_B(\boldsymbol{r})\big)+ P_C(\boldsymbol{r})\ln\big(P_C(\boldsymbol{r})\big)\Big] \end{aligned} \tag{2}$$

where $V_{\alpha\beta}(\boldsymbol{r}-\boldsymbol{r}')$ is the effective interchange interaction energy between α and β (α, β=A, B or C), including chemical interaction $V_{\alpha\beta}(\boldsymbol{r}-\boldsymbol{r}')_{at}$ and elastic interaction $V_{\alpha\beta}(\boldsymbol{r}-\boldsymbol{r}')_{el}$[12]:

$$V_{\alpha\beta}(\boldsymbol{r}-\boldsymbol{r}')=V_{\alpha\beta}(\boldsymbol{r}-\boldsymbol{r}')_{at}+V_{\alpha\beta}(\boldsymbol{r}-\boldsymbol{r}')_{el} \tag{3}$$

For chemical interaction $V_{\alpha\beta}(\boldsymbol{r}-\boldsymbol{r}')_{at}$, considering atom interaction up to the fourth neighbor, owing to the transition and possible arrangement of three kinds of atoms in ternary system, there are much more precise in the description of free energy.

$V^1_{\alpha\beta}$, $V^2_{\alpha\beta}$, $V^3_{\alpha\beta}$, $V^4_{\alpha\beta}$ represent the first, second, third and fourth nearest-neighbor interaction energy parameter, respectively. In the reciprocal space, the following equation is given:

$$\begin{aligned} V_{\alpha\beta}(\boldsymbol{k})_{at}=&4V^1_{\alpha\beta}(\cos\pi h\cdot\cos\pi k+\cos\pi h\cdot\cos\pi l+ \cos\pi k\cdot\cos\pi l)+2V^2_{\alpha\beta}(\cos2\pi h+\cos2\pi k+ \cos2\pi l)+8V^3_{\alpha\beta}(\cos2\pi h\cdot\cos\pi k\cdot\cos\pi l+ \cos\pi h\cdot\cos2\pi k\cdot\cos\pi l+\cos\pi h\cdot\cos\pi k\cdot \cos2\pi l)+4V^4_{\alpha\beta}(\cos2\pi h\cdot\cos2\pi k+ \cos2\pi h\cdot\cos2\pi l+\cos2\pi k\cdot\cos2\pi l) \end{aligned} \tag{4}$$

According to the Refs.[8,13], the following interaction parameters are used: for Ni and Al interactions (meV/atom), V_1=122.30, V_2=6.0, V_3=16.58, and V_4=−6.82; for Ni and Cr interactions (meV/ atom), V_1=84.8, V_2=−46.8, V_3=−10.4, and V_4=33.2; and for Al and Cr interactions (meV/atom), V_1=140, V_2=−40, V_3=−74.5, and V_4=0.

After Fourier transform and long wave approximation, the function $V(\boldsymbol{k})_{el}$ in 2D model could be written as

$$V(\boldsymbol{k})_{el}\approx B(\boldsymbol{e})\approx B(\boldsymbol{e}_x^2\boldsymbol{e}_y^2-0.125) \tag{5}$$

where $\boldsymbol{e}_x$ and $\boldsymbol{e}_y$ are components of the unit vector $\boldsymbol{e}$ along the x and y axes in the reciprocal space and

$$B=-\frac{4(c_{11}+2c_{12})}{c_{11}(c_{11}+c_{12}+2c_{44})}{\varepsilon_0}^2\Delta \tag{6}$$

where B is a material constant, which characterizes the elastic properties and the crystal lattice mismatch. $\Delta=c_{11}-c_{12}-2c_{44}$, is the elastic anisotropy constant. In this simulation, $B>0$, which occurs for alloys with a negative elastic anisotropy.

Substituting Eqns.(3), (4), (5) and (6) to (2) and (2) to (1) yields a reciprocal space representation of the ternary kinetic equation:

$$\begin{aligned} \frac{\mathrm{d}\tilde{P}_A(\boldsymbol{k},t)}{\mathrm{d}t}=&\frac{\tilde{L}_{AA}(\boldsymbol{k})}{\boldsymbol{k}_BT}\Big\{\tilde{V}_{AC}(\boldsymbol{k})\tilde{P}_A(\boldsymbol{k},t)+\frac{1}{2}\Big[-\tilde{V}_{AB}(\boldsymbol{k})+\tilde{V}_{BC}(\boldsymbol{k})+\tilde{V}_{AC}(\boldsymbol{k})\Big]\cdot \tilde{P}_B(\boldsymbol{k},t)\Big\}+\tilde{L}_{AA}(\boldsymbol{k})\left[\ln\frac{P_A(r,t)}{1-P_A(r,t)-P_B(r,t)}\right]_{\boldsymbol{k}}+\frac{\tilde{L}_{AB}(\boldsymbol{k})}{k_BT}\cdot \\ &\Big\{\tilde{V}_{BC}(\boldsymbol{k})\tilde{P}_B(\boldsymbol{k},t)+\frac{1}{2}\Big[-\tilde{V}_{AB}(\boldsymbol{k})+\tilde{V}_{BC}(\boldsymbol{k})+\tilde{V}_{AC}(\boldsymbol{k})\Big]\cdot \tilde{P}_A(\boldsymbol{k},t)\Big\}+\tilde{L}_{AB}(\boldsymbol{k})\left[\ln\frac{P_B(\boldsymbol{r},t)}{1-P_A(\boldsymbol{r},t)-P_B(\boldsymbol{r},t)}\right]_{\boldsymbol{k}}+\xi(\boldsymbol{k},t) \\ \frac{\mathrm{d}\tilde{P}_B(\boldsymbol{k},t)}{\mathrm{d}t}=&\frac{\tilde{L}_{BA}(\boldsymbol{k})}{\boldsymbol{k}_BT}\Big\{\tilde{V}_{AC}(\boldsymbol{k})\tilde{P}_A(\boldsymbol{k},t)+\frac{1}{2}\Big[-\tilde{V}_{AB}(\boldsymbol{k})+\tilde{V}_{BC}(\boldsymbol{k})+\tilde{V}_{AC}(\boldsymbol{k})\Big]\cdot \tilde{P}_B(\boldsymbol{k},t)\Big\}+\tilde{L}_{BA}(\boldsymbol{k})\cdot\left[\ln\frac{P_A(\boldsymbol{r},t)}{1-P_A(\boldsymbol{r},t)-P_B(\boldsymbol{r},t)}\right]_{\boldsymbol{k}}+\frac{\tilde{L}_{BB}(\boldsymbol{k})}{\boldsymbol{k}_BT}\cdot \\ &\Big\{\tilde{V}_{BC}(\boldsymbol{k})\tilde{P}_B(\boldsymbol{k},t)+\frac{1}{2}\Big[-\tilde{V}_{AB}(\boldsymbol{k})+\tilde{V}_{BC}(\boldsymbol{k})+\tilde{V}_{AC}(\boldsymbol{k})\Big]\cdot \tilde{P}_A(\boldsymbol{k},t)\Big\}+\tilde{L}_{BB}(\boldsymbol{k})\left[\ln\frac{P_B(\boldsymbol{r},t)}{1-P_A(\boldsymbol{r},t)-P_B(\boldsymbol{r},t)}\right]_{\boldsymbol{k}}+\xi(\boldsymbol{k},t) \end{aligned} \tag{7}$$

where $\tilde{P}_A(\boldsymbol{k},t)$, $\tilde{P}_B(\boldsymbol{k},t)$, $\tilde{L}_{AA}(\boldsymbol{k})$, $\tilde{L}_{AB}(\boldsymbol{k})$, $\tilde{L}_{BA}(\boldsymbol{k})$, $\tilde{L}_{BB}(\boldsymbol{k})$, $\xi(\boldsymbol{k},t)$, $V_{AB}(\boldsymbol{k})$, $V_{BC}(\boldsymbol{k})$, $V_{AC}(\boldsymbol{k})$, $\left[\ln\dfrac{P_A(\boldsymbol{r},t)}{1-P_A(\boldsymbol{r},t)-P_B(\boldsymbol{r},t)}\right]_{\boldsymbol{k}}$,

$\left[\ln\frac{P_B(\boldsymbol{r},t)}{1-P_A(\boldsymbol{r},t)-P_B(\boldsymbol{r},t)}\right]_{\boldsymbol{k}}$ are Fourier transform of corresponding functions in the real space.

Transform equation (7) from a 3D and a non-linear partial differential equation into a 2D and linear constant differential equation, thus, the computation work can be greatly decreased. The equation is solved by Euler method; and the atomic figures and order parameters at different time are obtained from the atomic occupation probabilities.

3 Results and discussion

In this simulation, real time is represented by simulation time, the time step Δt=0.000 2, and 256×256 lattices are used. The precipitation phases are denoted by different shades of gray. White, black and gray represent chromium, nickel and aluminum atom, respectively. If the occupation probability of chromium atom is 1.0, then that site is white, and so on. Therefore, the DO_{22} (Ni_3Cr) phase appears to be white, the $L1_2$ phase (Ni_3Al) appears to be gray and a black background is formed. In addition, the phase structure can also be identified by arrangement style of atoms on 2D projection plane[14]. The precipitation process of $Ni_{75}Al_9Cr_{16}$ alloy during two-step aging is simulated, in which the pre-aging temperatures are 873 K and 973 K, respectively, and re-aging temperatures are both at 1000 K; the pre-aging times are both 10 000 time steps, and the total times are both 1 000 000 time steps. The initial state of alloy is the disordered solid solution, and nucleation occurs by adding certain thermal noise, then, thermal noise is removed, and the system spontaneously selects kinetics paths. The pre-aging temperature effects on the precipitation mechanism and microstructure are analyzed by the acquired atomic figures and order parameters.

Fig.1 shows the atomic morphology evolution for $Ni_{75}Al_9Cr_{16}$ alloy during two-step aging from 873 K to

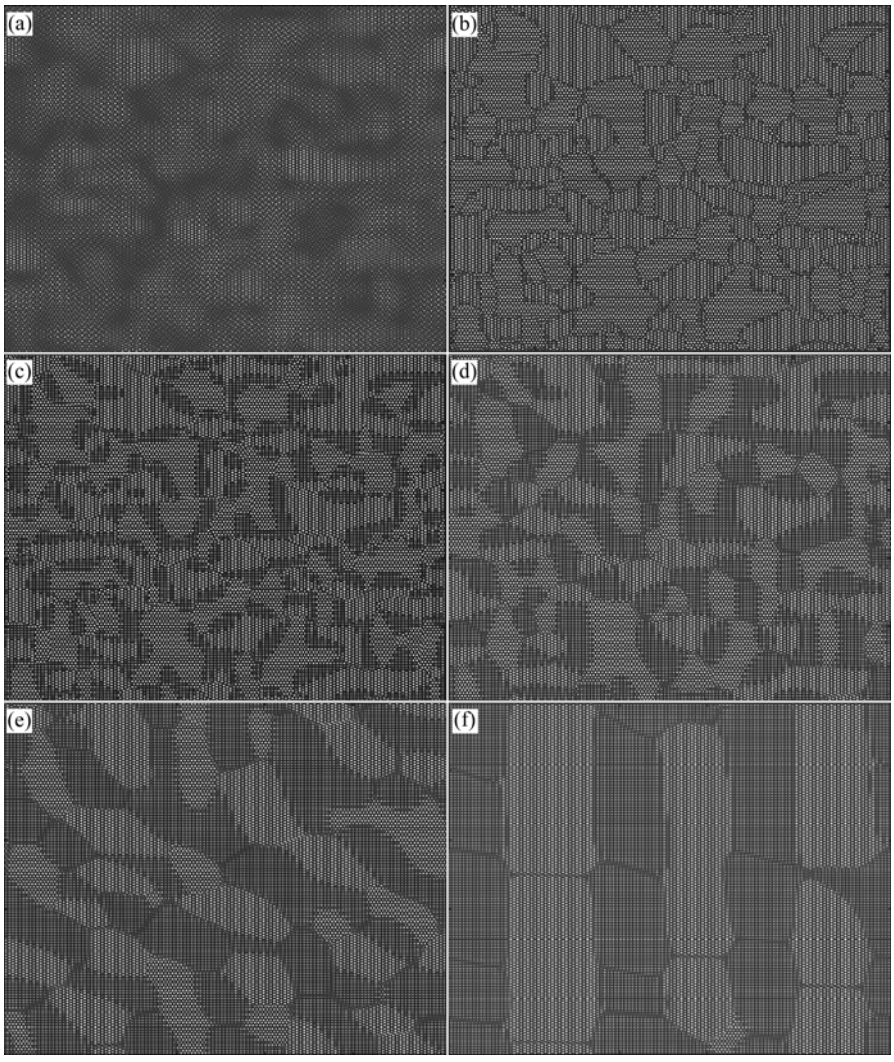

Fig.1 Atom morphology evolution for $Ni_{75}Al_9Cr_{16}$ alloy during two-step aging from 873 K to 1 000 K: (a) t=1 800; (b) t=3 000; (c) t= 10 000; (d) t=50 000; (e) t=200 000; (f) t=1 000 000

1000 K. The saturation degree of alloy is relatively higher due to the lower pre-aging temperature, so the precipitated phases rapidly appear in the disordered matrix at 1 800 time step as shown in Fig.1(a). According to the color and 2D projection of the atoms, it can be concluded that they are DO_{22} phases. Fig.1(b) shows the atomic picture at 3 000 time step, from which we can clearly see that the DO_{22} phases begin to grow, and the amount of DO_{22} phases fiercely increases in short time, simultaneously, followed by the appearance of a few $L1_2$ ordered phases at the APBs of the DO_{22} phases. The fact that $L1_2$ phases tend to form at the APBs of DO_{22} phases arises from the appearance of Cr-rich zone because of solute atom diffusion. The atomic pictures at 10 000 and 50 000 time step are shown in Fig.1(c), and Fig.1(d), respectively. It can be seen that $L1_2$ phases grow at the phase boundary of DO_{22} phases; at the same time, the amount of DO_{22} phases begins to decrease. The DO_{22} phases of low ordering degree transform into $L1_2$ phases owing to the diffusion of atoms, and the increase of $L1_2$ phases corresponds to the decrease of DO_{22} phases. With aging progressing, the DO_{22} and $L1_2$ phase particles begin to collide and merge, which is accompanied with interfacial migration. In this process, the smaller particles become smaller and smaller and finally vanish, while the larger particles become larger and larger, and the spacing interval of both the DO_{22} and $L1_2$ phases become larger and larger. Fig.1(e) and Fig.1 (f) show the atomic pictures at 200 000 and 1 000 000 time step, respectively, from which we can see that the DO_{22} and $L1_2$ phase particles change from random shape at the early stage to cubic shape at the late stage, and the arrangement of DO_{22} and $L1_2$ phase particles becomes more and more regular. Finally, the equilibrium two-phase mixture is formed, in which DO_{22} and $L1_2$ phases are aligned along [100] and [010] directions, i.e. elastically soft directions.

The laws of formation, growth, coarsening and distribution of precipitated phases can be clearly seen from the atomic morphology evolution. However, it's unreliable to judge the early precipitation mechanism only by the observation of atomic pictures. In order to clarify the early precipitation mechanism, the order parameters across the ordered phase are calculated. The early precipitation mechanism can be studied in depth by the law of order parameter evolvement across $L1_2$ and DO_{22} ordered phase, which is very difficultly carried out in experiments, however, can be easily achieved by computer simulation. Ordering coexists with atomic clustering during precipitation of alloy, which can be described by the long range order parameter and composition order parameter, respectively.

The evolutions of Cr composition order parameter and Cr long range order parameter across the DO_{22} phase for $Ni_{75}Al_9Cr_{16}$ alloy during two-step aging from 873 K to 1000 K are presented in Fig.2(a) and Fig.2(b) respectively. It can be seen that composition and long range order parameter both have slight fluctuation at 1 500 time step. The long range order parameter has reached the equilibrium value, while the composition order parameter is far below the equilibrium value at 3 000 time step, which illustrates the atomic clustering is later than its ordering process and formed precipitated phase is the non-stoichiometric ordered phase. Then, the composition order parameter gradually rises to equilibrium value. At this stage, the composition order parameter shows the characteristic that its center is concave and the edge is prominent, which results from the diffusion of Cr solute atoms along phase boundary, thus, the Cr solute atoms become poor in the center of DO_{22} ordered phase. When the diffusion of solute atoms continues, the center of composition order parameter finally reaches the equilibrium value. On the whole, the order parameter evolution of DO_{22} phase shows the trait of spinodal decomposition along with small fluctuation in large region. So, it can be concluded from the simulation

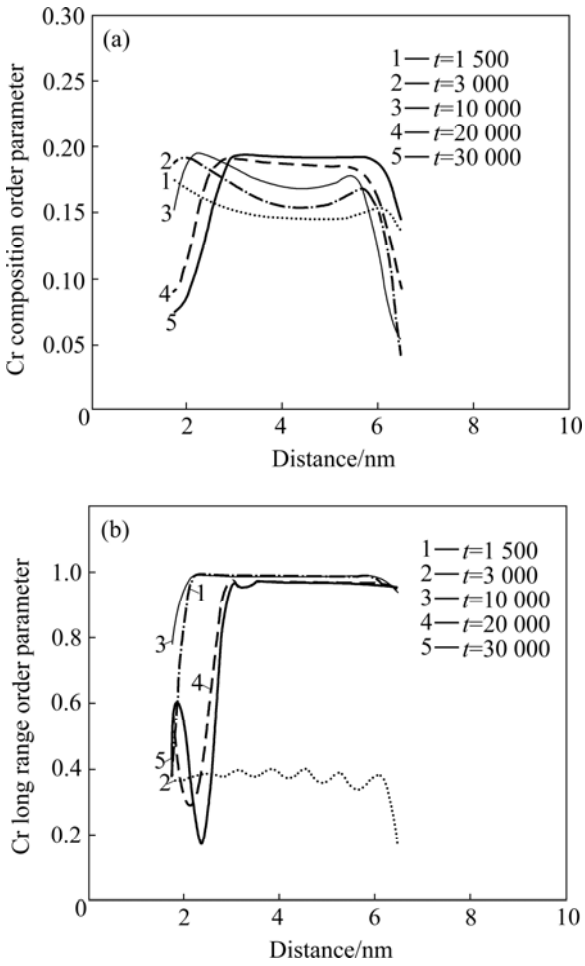

Fig.2 Evolution of Cr composition order parameter (a) and Cr long range order parameter (b) across DO_{22} phase for $Ni_{75}Al_9Cr_{16}$ alloy during two-step aging from 873 K to 1 000 K

that the early precipitation mechanism of DO_{22} phase for $Ni_{75}Al_9Cr_{16}$ alloy during two-step aging from 873 K to 1 023 K is spinodal decomposition.

Fig.3 shows the evolution of Al composition order parameter (a) and Al long range order parameter (b) across the $L1_2$ phase for $Ni_{75}Al_9Cr_{16}$ alloy during two-step aging from 873 K to 1 000 K. The composition order parameter and long range order parameter both have slight fluctuation, but do not reach the equilibrium value at 2 500 time step. Then, the long range order parameter rises faster than the composition order parameter, i.e. the atomic ordering is faster than its clustering. The composition order parameter reaches the equilibrium value, while the long range order parameter is far below the equilibrium value at 3 200 time step; at the same time, the composition order parameter becomes wider and wider with aging progressing. At this stage, the evolution of composition order parameter demonstrates the traits of non-classical nucleation and growth that the composition order parameter doesn't reach the equilibrium initially, and the phase boundary belongs to disperse interface. With continual aging, the evolution of order parameter shows the trait of spinodal

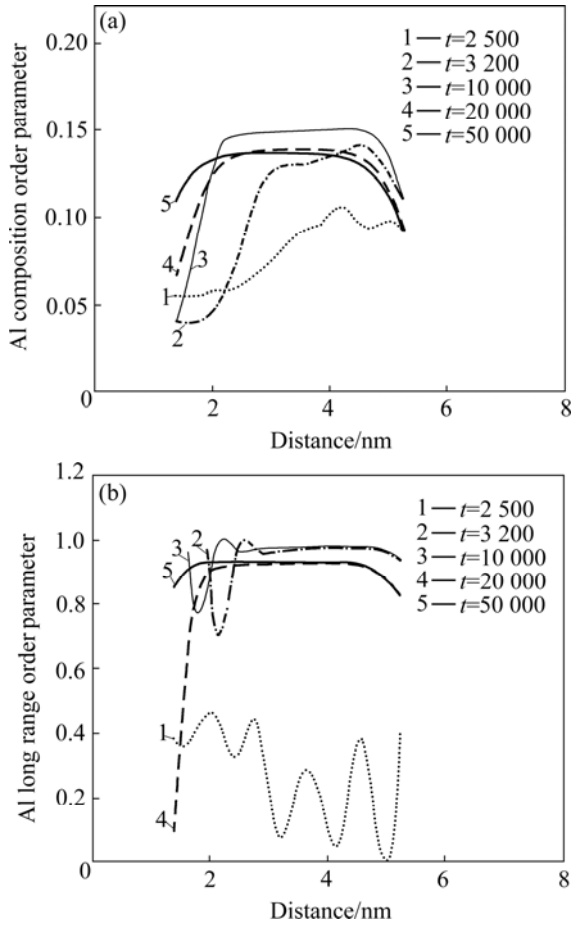

Fig.3 Evolution of Al composition order parameter (a) and Al long range order parameter (b) across $L1_2$ phase for $Ni_{75}Al_9Cr_{16}$ alloy during two-step aging from 873 K to 1 000 K

decomposition that the composition order parameter width keeps invariable and its height becomes higher and higher up to the equilibrium value. From the above simulation, it is concluded that the early precipitation mechanism of $L1_2$ phase for $Ni_{75}Al_9Cr_{16}$ during two-step aging from 873 K to 1023 K is the mixed mechanism of non-classical nucleation growth and spinodal decomposition.

Fig.4 presents the atomic morphology evolution for $Ni_{75}Al_9Cr_{16}$ alloy during two-step aging from 973 K to 1 000 K. Compared with the state of pre-aging temperature of 873 K, the driving force of transformation decreases, and the nucleation incubation time becomes longer because the saturation degree of alloy decreases at higher pre-temperature. As shown in Fig.4(a), some DO_{22} phases appear at 4 400 time step, which are fewer in quantity and larger in size than those of pre-aging temperature of 873 K. $L1_2$ phases appear at the DO_{22} phase boundary at 5 000 time step as presented in Fig.4(b), and then, the evolution trait of atomic pictures as shown in Figs.4(c)−(f) is similar to that of pre-aging temperature of 873 K, that is, some DO_{22} phases transform into $L1_2$ phases, and finally the equilibrium two-phase mixture of DO_{22} and $L1_2$ ordered phases are aligned along the [100] and [010] directions. The DO_{22} and $L1_2$ phase particle arrangement along the elastically soft direction is not more obvious than that of pre-aging temperature of 873 K, which demonstrates the pre-aging temperature has evident influence on the microstructure of alloy during two-step aging.

Fig.5 shows the evolution of Cr composition order parameter and Cr long range order parameter across the DO_{22} phase for $Ni_{75}Al_9Cr_{16}$ alloy during two-step aging from 973 K to 1 000 K. The evolution trait is similar to that of pre-aging temperature of 873 K except that the precipitation incubation becomes longer. From the simulation results, we can conclude that the early precipitation mechanism of DO_{22} phase for $Ni_{75}Al_9Cr_{16}$ alloy during two-step aging from 973 K to 1 023 K is also spinodal decomposition.

The evolution of Al composition order parameter (a) and Al long range order parameter (b) across the $L1_2$ phase for $Ni_{75}Al_9Cr_{16}$ alloy during two-step aging from 973 K to 1 000 K are presented in Fig.6. The composition order parameter and long range order parameter both have slight fluctuation at 5 000 time step, and then they begin to rise together. At this stage, the composition order parameter and long range order parameter both show the characteristic that its center is high and the edge is low, and the center of order parameter slowly rises to equilibrium value. Then the height of order parameter keeps invariant, but the order parameter becomes wider and wider with progressing of aging, which corresponds to the growth of $L1_2$ phase. There

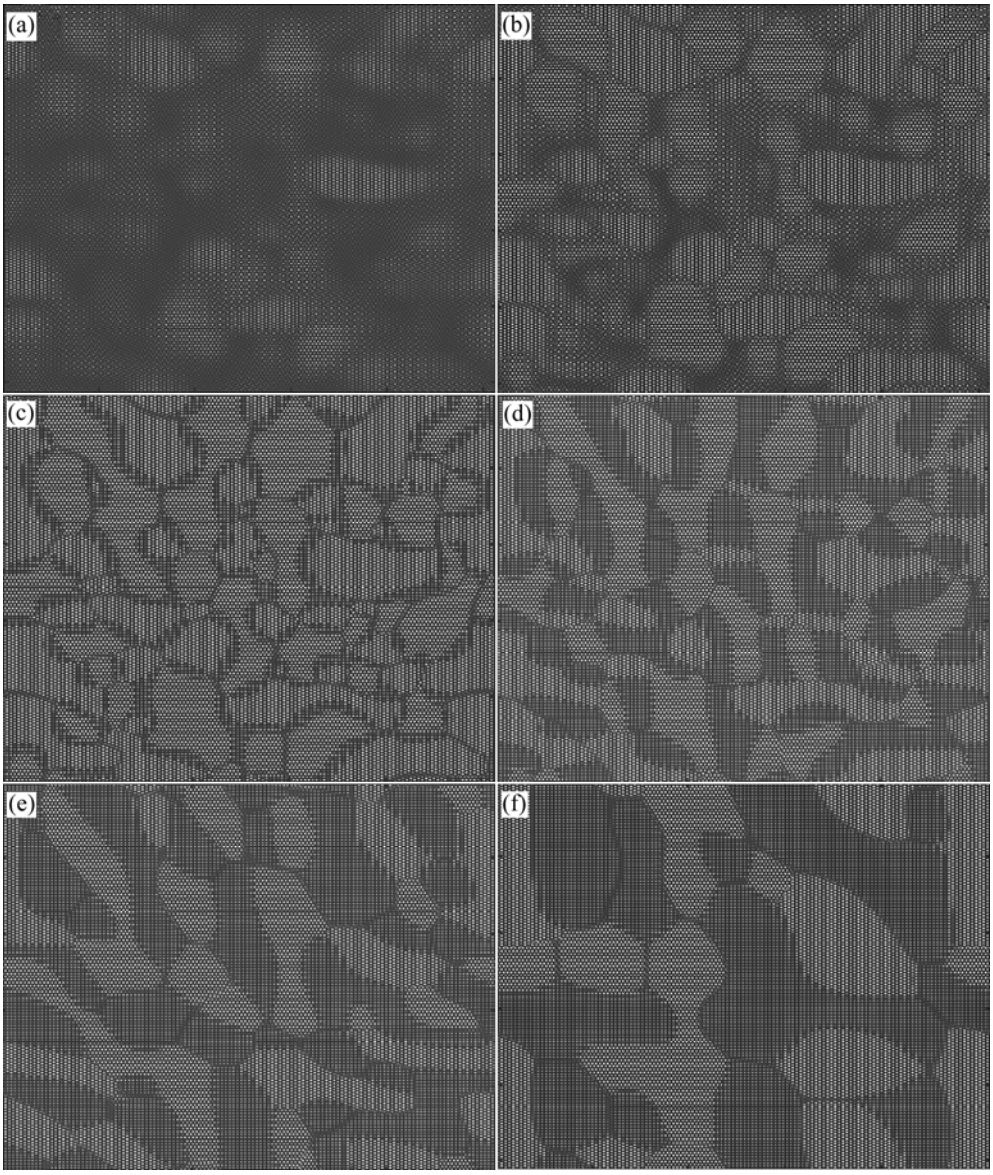

Fig.4 Atom morphology evolution for $Ni_{75}Al_9Cr_{16}$ alloy during two-step aging from 973 K to 1 000 K: (a) t=4 400; (b) t=5 000; (c) t= 10 000; (d) t=50 000; (e) t=200 000; (f) t=1 000 000

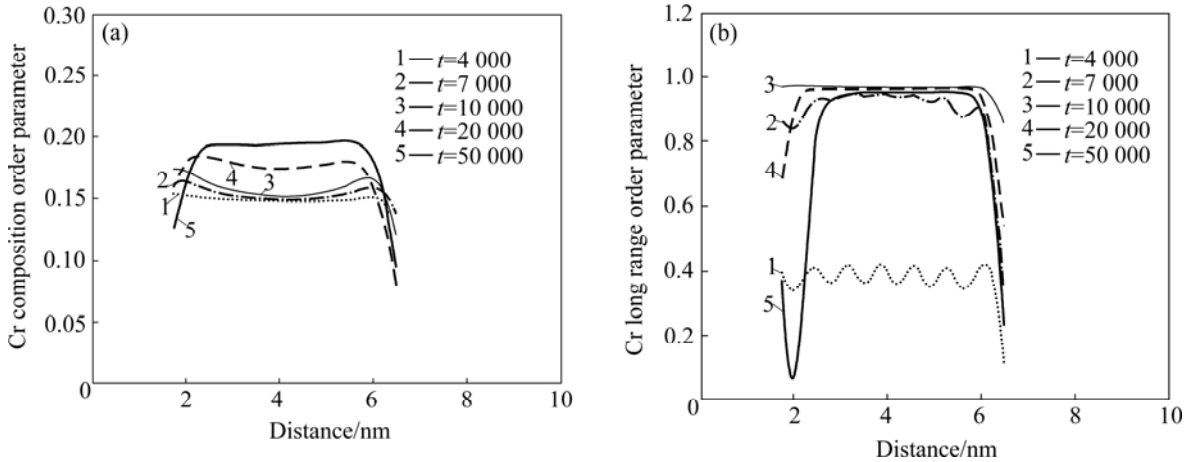

Fig.5 Evolution of Cr composition order parameter (a) and Cr long range order parameter (b) across DO_{22} phase for $Ni_{75}Al_9Cr_{16}$ alloy during two-step aging from 973 K to 1 000 K

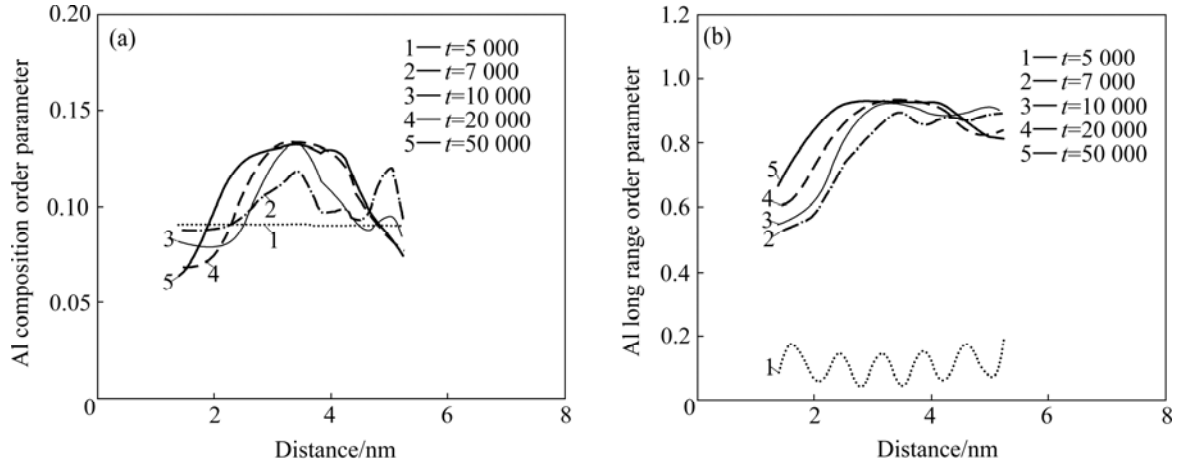

Fig.6 Evolution of Al composition order parameter (a) and Al long range order parameter (b) across $L1_2$ phase for $Ni_{75}Al_9Cr_{16}$ alloy during two-step aging from 973 K to 1 000 K

also exists some extension degree at the phase boundary which belongs to disperse interface. That above is the characteristic of the non-classical nucleation and growth, so, it can be concluded from the simulation that the early precipitation mechanism of $L1_2$ phase is non-classical nucleation and growth.

In general, the pre-aging temperature has some influence on the mechanism of precipitation for $Ni_{75}Al_9Cr_{16}$ alloy during two-step aging. The early precipitation mechanism of $L1_2$ phase changes from mixed mechanism of non-classical nucleation and growth and spinodal decomposition to non-classical nucleation and growth with the increase of pre-aging temperature from 873 K to 973 K. However, the early precipitation mechanism of DO_{22} phase keeps spinodal decomposition all along. The pre-aging temperature influence on nucleation incubation time has two sides. On one hand, the lower pre-temperature results in the higher saturation degree of alloy and faster nucleation speed rate, which is advantageous to the shortening of incubation time; on the other hand, the lower pre-temperature also induces the lower atomic diffusion coefficient, which makes incubation time longer. The simulation in this work reveals that the incubation time is longer at lower temperature, which demonstrates the first influence factor is the dominant factor on the incubation time.

Simultaneously, the simulation shows that the elastic energy has remarkable influence on microstructure for $Ni_{75}Al_9Cr_{16}$ alloy during two-step aging. In the early precipitation, because of the slight influence of elastic energy, the $L1_2$ phases and DO_{22} phases are randomly distributed in the matrix. With aging progressing, the misfit degree of lattice between the precipitated phase and matrix increases, so the elastic energy becomes larger and larger. The decrease of the sum of surface energy and elastic energy is the driving force of coarsening at the latter stage of precipitation, and the shape and distribution of precipitated phase depend both on the competition and harmonization of them. The theoretical calculations in Ref.[15] testify that precipitated phase arrangement along [100] and [010] directions tends to have lower energy in Ni-Al system. Fig.7 shows the comparison between simulated morphology and experimental result in Ref.[16]. Ni-Al-Cr alloy and Ni-Al-Ti alloy are both Ni-based alloys. We

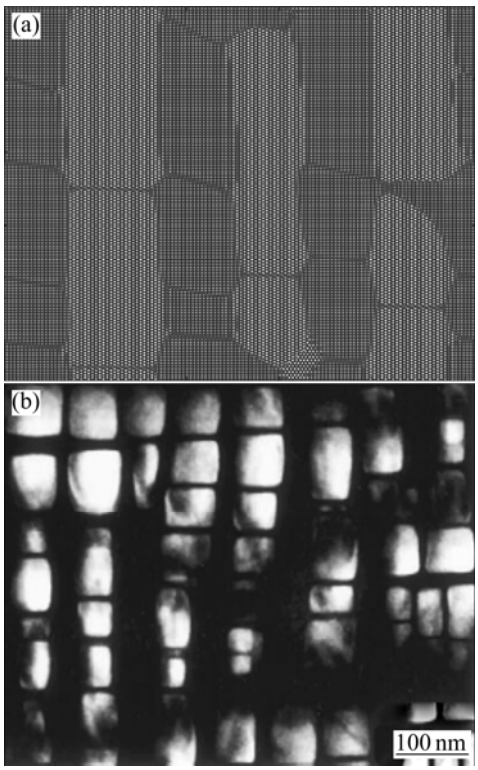

Fig.7 Comparison of simulated morphology in $Ni_{75}Al_9Cr_{16}$ alloy and experimental results: (a) Simulated morphology for $Ni_{75}Al_9Cr_{16}$ alloy aged at 873 K and 1 000 K; (b) Dark field image of γ' phase in Ni-8Al-6Ti alloy aged at 1023 K for 1.728 $\times 10^5$ s

can clearly see that these two kinds of morphologies are generally alike during the latter precipitation, and they both arrange along [100] and [010] directions. In addition, LUND and VOORHEES[17] found the $L1_2$ phases arrangement along the **<100>** direction at the latter stage of precipitation in the Ni-Al system. NUNOMURA et al[18] also found similar arrangement of $L1_2$ and DO_{22} phases in the pseudo-ternary Ni_3Al-Ni_3Ti-Ni_3V system in their experiments. This work reveals that the $L1_2$ phases and DO_{22} phases tend to be cuboidal arrangement along the [100] and [010] directions, which is more obvious at the lower pre-temperature.

4 Conclusions

1) Pre-aging temperature has evident influence on the early precipitation mechanism for $Ni_{75}Al_9Cr_{16}$ alloy during two-step aging. With the increase of pre-temperature, the early precipitation mechanism of $L1_2$ phase changes from mixed mechanism of non-classical nucleation growth and spinodal decomposition to non-classical nucleation growth; and the early precipitation mechanism of DO_{22} phase is still spinodal decomposition.

2) The shape of precipitated phase is heavily influenced by the elastic energy at the latter stage of precipitation. The $L1_2$ and DO_{22} phases tend to arrange along the [100] and [010] directions, which is more obvious at the lower pre-temperature.

3) During these two kinds of two-step aging, DO_{22} phases appear earlier than $L1_2$ phases, then $L1_2$ phases begin to form at the APBs of DO_{22} phases, and the nucleation incubation time becomes long with the increase of pre-temperature.

References

[1] SUDBRACK C K, YOON K E, NOEBE R D, SEIDMAN D N. Temporal evolution of the nanostructure and phase compositions in a model Ni-Al-Cr alloy [J]. Acta Mater, 2006, 54(12): 3199−3210.

[2] FISCHER R, ELENO L T F, FROMMEYER G, SCHNEIDER A. Precipitation of Cr-rich phases in a Ni-50Al-2Cr (at.%) alloy [J]. Intermetallics, 2006, 14(2): 156−162.

[3] LAPIN J, VAŇO A. Coarsening kinetics of α and γ'-precipitates in a multiphase intermetallic Ni-Al-Cr-Ti type alloy with additions of Mo and Zr [J]. Scripta Mater, 2004, 50(5): 571−575.

[4] PICHA R, BROŽ P, BURŠÍK J. Phase equilibria in the Ni-Al-Cr-Ti system at 1 000 and 1 100 ℃ [J]. J Alloys Compd, 2004, 378(1/2): 75−78.

[5] BROŽ P, SVOBODA M, BURŠÍK J, KROUPA A, HAVRÁNKOVÁ J. Theoretical and experimental study of the influence of Cr on the γ+γ' phase field boundary in the Ni-Al-Cr system [J]. Mater Sci Eng, A, 2002, A325(1/2): 59−65.

[6] PODURI R, CHEN L Q. Computer simulation of the kinetics of order-disorder and phase separation during precipitation of δ' (Al_3Li) in Al-Li alloys [J]. Acta Mater, 1997, 45(1): 245−255.

[7] LU Yan-li, CHEN Zheng, LI Yong-sheng, WANG Yong-xin. Microscopic phase-field simulation for Ni_3Al precipitation in Ni-Al alloy [J]. Acta Metallurgica Sinica, 2007, 43(3): 291−296.

[8] PODURI R, CHEN L Q. Computer simulation of atomic ordering and compositional clustering in the pseudobinary Ni_3Al-Ni_3V system [J]. Acta Mater, 1998, 46(5): 1719−1729.

[9] LI Yong-sheng, CHEN Zheng, WANG Yong-xin, LU Yan-li. Computer simulation of γ' and θ phase precipitation of Ni-Al-V alloy using microscopic phase-field method [J]. Trans Nonferrous Met Soc China, 2005, 15(1): 57−63.

[10] LI Yong-sheng, CHEN Zheng, LU Yan-li, WANG Yong-xin. Phase-field simulation of phase separation in $Ni75Al_xV_{25-x}$ alloy with elastic stress [J]. Trans Nonferrous Met Soc China, 2006, 16(3) 2017−2021.

[11] KHACHATURYAN A G. Theory of structural transformation in solids [M]. New York: Wiley, 1983: 129−136.

[12] ONUKI A. Ginzburg-Landau approach to elastic effects in the phase separation of solids [J]. J Phys Soc Jpn, 1989, 58: 3065−3068.

[13] PAREIGE C, SOISSON F, MARTIN G, BLAVETTE D. Ordering and phase separation in Ni-Cr-Al: Monte Carlo simulations vs three-dimensional atom probe [J]. Acta Mater, 1999, 47(6): 1889−1899.

[14] DUVAL S, CHAMBRELAND S, CARON P, BLAVETTE D. Phase composition and chemical order in the single crystal nickel base superalloy MC2 [J]. Acta Metal Mater, 1994, 42(1): 185−194.

[15] DOI M. Elasticity effects on the microstructure of alloys containing coherent precipitates [J]. Progress in Materials Science, 1996, 40(2): 79−180.

[16] MAEBASHI T, DOI M. Coarsening behaviours of coherent γ' and γ precipitates in elastically constrained Ni-Al-Ti alloys [J]. Mater Sci Eng A, 2004, 373(1/2): 72−79.

[17] LUND A C, VOORHEES P W. The effects of elastic stress on coarsening in the Ni-Al system [J]. Acta Mater, 2002, 50(8): 2085−2098.

[18] NUNOMURA Y, KANENO Y, TSUDA H, TAKASUGI. Phase relation and microstructure in multi-phase intermetallic alloys based on Ni_3Al-Ni_3Ti-Ni_3V pseudo-ternary alloy system [J]. Intermetallics, 2004, 12(4): 389−399.

(Edited by YANG Bing)